Positron wave-function effects in the measurement of the two-dimensional angular correlation of the annihilation radiation of a spin-polarized system

Ján Rusz*
Department of Physics, Uppsala University, Box 530, S-751 21 Uppsala, Sweden
and Institute of Physics, Academy of Sciences of the Czech Republic, Na Slovance 2, 182 21 Prague 8, Czech Republic.

Maurizio Biasini†
Department of Physics, University of California at Riverside, Riverside, California 92521, USA
(Received 11 December 2006; revised manuscript received 6 March 2007; published 19 June 2007)

In positron annihilation studies of the electronic structure of metals, a nonuniform positron density can distort significantly the faithful detection of the Fermi surface. Recently, we have predicted a nearly complete cancellation of the aforementioned distortion in the spin-polarized two-dimensional angular correlation of annihilation radiation experiment on CrO_2 [M. Biasini and J. Rusz, J. Phys.: Condens. Matter **18**, L289 (2006)]. We provide a detailed investigation of the predicted effect on several transition-element- and actinide-based systems of increasing complexity, demonstrating that the cancellation effect is of rather general nature.

DOI: 10.1103/PhysRevB.75.235115 PACS number(s): 71.18.+y, 71.27.+a, 71.60.+z, 78.70.Bj

I. INTRODUCTION

With the development of more reliable and sophisticated methods to reconstruct the three-dimensional (3D) Fermi surface (FS) of metals,[1,2] the positron annihilation technique, by measuring the two-dimensional angular correlation of the electron-positron annihilation radiation (2D-ACAR), is the only tool able to provide 3D views of the FS of truly three-dimensional systems.[3–5] Other practical advantages of the 2D-ACAR experiment are that it is relatively insensitive to surface degradation, it can be performed at any temperature (at the expense of a modest degradation in the experimental resolution), thus monitoring the onset of magnetic and/or charge orderings, and it can be performed on alloys characterized by compositional disorder.

On the other hand, a renowned drawback of 2D-ACAR is the possible disturbance introduced by the electron-positron correlations[6–10] and by the selective sampling of the electronic states caused by the nonuniform positron density (often denoted as positron wave-function effect, or simply *probe effect*). Although both phenomena are, in general, noteworthy, it is the positron wave-function effect which in important cases, such as some high-T_C superconductors and itinerant 5*f*-electron systems, has almost wiped out the information on the Fermi surface.[11,12]

In this work, we will show that by a carefully performed experiment on ferromagnetic samples, it should be possible to eliminate a large part of the probe effect. Our first results on the cancellation of the probe effects have been published in Ref. 13. In this work, we extend these studies by a more detailed analysis of the cancellation, predicted for several transition-element- and actinide-based compounds.

The structure of this work is as follows: in Sec. II, we describe theoretical methods used for calculation of the (reduced) electron-positron momentum density. In Sec. III, we describe results of our calculations on the transition-metal-based CrO_2, NiMnSb, and Ni_2MnSb compounds and on the actinide-based compound UGe_2. Section IV contains the summary and concluding remarks.

II. THEORETICAL METHODS

A. Momentum density of annihilating pairs

By measuring the distribution $N(\theta_x,\theta_y)$ of the deviation angles from anticollinearity of the annihilation γ rays, a 2D-ACAR experiment determines a two-dimensional (2D) projection of the 3D electron-positron (*ep*) momentum density $\rho^{ep}(\mathbf{p})$,[14] which can be expressed in the single-particle approximation as

$$\rho^{2\gamma}(\mathbf{p}) \propto \sum_{n,\mathbf{k}}^{occ} \left| \int d\mathbf{r}\, \exp(-i\mathbf{p}\cdot\mathbf{r})\psi_{\mathbf{k}}^{n}(\mathbf{r})\phi^{\star}(\mathbf{r})\sqrt{g(\mathbf{r})} \right|^2. \quad (1)$$

Here, $\psi_{\mathbf{k}}^{n}$ and ϕ denote the electron and positron wave function, respectively, and the summation extends over all occupied $\mathbf{k}$ electron states from bands of index n.[14] The enhancement factor[15] $g(\mathbf{r})$, function of the total electronic density $n(\mathbf{r})$ $\{g(\mathbf{r})\equiv g[n(\mathbf{r})]\}$, describes the enhancement of the electronic density at the positron location due to the Coulomb force. The contribution to $\rho^{ep}(\mathbf{p})$ from the conduction bands l is discontinuous at points $\mathbf{p}_{F_l}=(\mathbf{k}_{F_l}+\mathbf{G})$, where $\mathbf{G}$ is a reciprocal-lattice vector and $\mathbf{k}_{F_l}$ are the reduced Fermi wave vectors in the first Brillouin zone (BZ). The standard Lock-Crisp-West (LCW) transformation[16] reinforces these discontinuities by folding the momentum distribution $\rho^{ep}(\mathbf{p})$ back onto the first BZ by translation over the appropriate vectors $\mathbf{G}$. The result of the summation, denoted as LCW density (or *reduced* electron-positron momentum density), is[17]

$$\rho_{LCW}^{ep}(\mathbf{k}) = \sum_{n} \theta(E_F-\epsilon_{\mathbf{k},n}) \int |\psi_{\mathbf{k}}^{n}(\mathbf{r})|^2 |\phi(\mathbf{r})|^2 g(\mathbf{r})\, d\mathbf{r}. \quad (2)$$

Here, ϕ, $\psi_{\mathbf{k}}^{n}$, and $g(\mathbf{r})$ have the same meaning as in Eq. (1), E_F is the Fermi level, and $\epsilon_{\mathbf{k},n}$ is the energy eigenvalue of the electron from band n with Bloch wave vector $\mathbf{k}$. If the $\mathbf{k}$, n dependence of the overlap integral in Eq. (2) is negligible, $\rho_{LCW}^{ep}(\mathbf{k})$ will be proportional to the *occupancy*, i.e., the number of occupied states per $\mathbf{k}$ point. The FS manifolds are the loci of the discontinuities of the occupancy. Note that the 3D

LCW transformation is performed after $\rho^{ep}(\mathbf{p})$ is reconstructed tomographically on the base of its 2D projections.[1,2]

In Refs. 12 and 18, we have presented a method to calculate directly the LCW density via Eq. (2). The method, which is faster and computationally simpler than the calculation of $\rho^{ep}(\mathbf{p})$ via Eq. (1), implies that the LCW folding of the experimental spectrum has been performed over a sufficient portion of momentum space. As a base for our calculation, we used the full-potential linearized augmented plane-wave (FLAPW) method implemented in the WIEN2K package.[19] Compared to similar works of other authors,[17,20] our scheme, being *full potential* and compatible with any option of WIEN2K, which include spin-orbit interaction, LDA+U, and orbital polarization, is more suited to the study of narrow bands and electron correlations. Electron-positron correlation effects are included adopting the theory developed by Boronski and Nieminen[15] which, despite its simplicity, has recently been confirmed to be a very effective recipe to study metallic systems.[21] We also recall that the positron wave function is calculated replacing the electron potential [consisting of the Coulombic potential $V_{Coul}(\mathbf{r})$, arising from the nuclei and from the Hartree potential of the electron density $n(\mathbf{r})$,[22] plus the exchange-correlation potential $V_{xc}(\mathbf{r})$] (Refs. 23 and 24) with the positron potential, constructed as the sum of the inverted $V_{Coul}(\mathbf{r})$ and the term due to the electron-positron enhancement (see Ref. 15). Indeed, since the positron annihilation rate is much larger than typical radioactive source intensities, one can safely assume to have only one positron in the system, populating the lowest-energy band at the Γ point.

B. Spin-polarized systems

The employment of 2D-ACAR experiments to study magnetic substances[25–30] hinges on two findings. First, positrons emitted in the beta decay of various radioactive sources are produced with a helicity equal to v/c [recall that the helicity operator is $h=\Sigma\cdot\hat{\mathbf{p}}$, where Σ and $\hat{\mathbf{p}}$ are the spin and unit momentum ($\hat{\mathbf{p}}=\mathbf{p}/|\mathbf{p}|$) operators, respectively[31]]. For the most commonly employed radioactive source ^{22}Na, the end point energy of the beta spectrum is 540 keV and the average helicity is about 73%. If positrons from one side of the source are collected by the sample, the average polarization of the positrons P_{e^+} entering the sample [resulting from the angular average of $\cos(\theta)$ over a solid angle of 2π] will be about 36%. The positrons thermalize very rapidly in the sample, with little loss of polarization. Second, measurements are performed when the sample magnetization is saturated by an external magnetic field with directions, respectively, parallel and antiparallel to the average positron polarization (which is unchanged upon reversal of the magnetic field). The fractions of positrons antiparallel and parallel to the majority spins are then $n^{\uparrow}=\frac{1}{2}(1+P_{e^+})$ and $n^{\downarrow}=\frac{1}{2}(1-P_{e^+})$, respectively. Parity and angular momentum conservation require that the positron may undergo 2γ annihilation only if the spins of the annihilating pair form a singlet state. The two aforementioned measurements (with B parallel and antiparallel to the positron polarization) will then yield an observable imbalance of 2γ annihilations with respect to the majority or minority spins.

C. Cancellation of probe effects

Unlike the de Haas–van Alphen (dHvA) effect, where only the extremal cross-sectional orbits of the FS perpendicular to the applied magnetic field contribute to the quantum oscillations of the magnetization, in a 2D-ACAR experiment, all the outer electrons overlap with the positron probe. On the one hand, this feature can be advantageous since it allows us to study electronic states of semiconductors and insulators (where dHvA simply does not detect any oscillation). On the other hand, the contribution from the full bands and associated statistical noise can obscure the Fermi breaks. This drawback can be extremely relevant when the orbital character of one full valence band, caused by the specific degree of hybridization among the various orbital states (s,p,d,f), changes noticeably in the BZ. A $\mathbf{k}$-dependent orbital character controls essentially the amount of time spent by the electron in the interstitial region, where the positron resides prevalently due to its positive charge. Consequently, the positron generally samples states with strong d or f character much less compared to the highly delocalized s and p electrons. Therefore, the LCW density relative to the band in question acquires [via the overlap integral of Eq. (2)] a $\mathbf{k}$ dependence which is superimposed to the changes in the occupancy due to the FS breaks of the conduction bands. For example, our recent work on paramagnetic UGa_3 (Ref. 12) has detected a noticeable change in the p character of three valence bands located 1–2 eV below E_F which did obscure greatly the visibility of the FS.

In ferromagnetic transition-element-based and rare-earth-based compounds, the magnetic moments are carried mainly by the exchange-split d or f bands. The s and p bands remain essentially only weakly polarized with small hybridization-induced magnetic moments. This observation is essential in realizing that the contribution of the s,p bands to the momentum spin density will be rather similar for both spin orientations. Therefore, a signal contained in the *difference* of momentum densities measured for two orientations of the magnetic field will be predominantly due to exchange-split d or f bands. Surprisingly, this fact remained unnoticed. For example, in a comprehensive study of the half-metal NiMnSb, it appeared that the calculated[28] spin-momentum densities contain very similar features for both spin orientations in large areas of the Brillouin zones. However, this finding was not further commented.

Let us denote the up-spin bands the majority bands (N^M) and the down-spin bands the minority bands (N^m), respectively. The positron will then sample majority- and minority-spin bands according to the polarization fraction P_{e^+}. The experimental spectra taken when the positron polarization is parallel (antiparallel) to the polarizing magnetic field will be

$$\rho^{ep}_{par,antipar}(\mathbf{p}) = 1/2(1 \pm P_{e^+})[N^M(\mathbf{p}) + N^{NM}(\mathbf{p})/2] + 1/2(1 \mp P_{e^+})[N^m(\mathbf{p}) + N^{NM}(\mathbf{p})/2]. \quad (3)$$

In Eq. (3), we have separated the contribution, denoted as

N^{NM}, which comes from bands which are essentially nonpolarized or very weakly polarized, and thus do not contribute to the magnetism of a given compound (their exchange splitting is very small). We refer to N^{NM} as to the *nonmagnetic* part of the electron momentum density.[32]

Subtraction of ρ^{ep}_{par} from $\rho^{ep}_{antipar}$ yields the net momentum spin density $\rho^{ep}_{spin}(\mathbf{p})$.

$$\rho^{ep}_{spin}(\mathbf{p}) = P_{e^+}[N^M(\mathbf{p}) - N^m(\mathbf{p})]. \quad (4)$$

Equations (3) and (4) are equally applicable to the electron-positron momentum density $\rho^{ep}(\mathbf{p})$ or to the LCW density $\rho^{ep}_{LCW}(\mathbf{k})$.

In the examples considered in the next section, we will show that probe effects, which often plague the interpretation of the 2D-ACAR measurements, are strongly reduced in $\rho^{ep}_{spin}(\mathbf{p})$.

Note that the integrated difference between *normalized* experimental spectra $\rho^{ep\text{-}expt}_{par}$, $\rho^{ep\text{-}expt}_{antipar}$ yields zero by construction. This is in contrast with the integrated difference of the theoretical spin-momentum densities, which in the absence of probe effects, would be proportional to the total spin moment. To override this drawback of the experiment, different remedies have been proposed,[25–30] all based on some small renormalization of the experimental data prior to taking the difference $\rho^{ep\text{-}expt}_{par} - \rho^{ep\text{-}expt}_{antipar}$. In any case, the FS related discontinuities are not shifted by any renormalization of the spectra.

III. RESULTS

In this section, we provide several examples of the cancellation conjectured in the previous section. Firstly, we extend the study[13] of the half-metallic CrO_2 by discussing in more detail the reasons for the predicted nearly perfect cancellation of the positron wave-function effect.

Next, we turn to a comparative analysis of the NiMnSb and Ni_2MnSb Heusler alloys which, in spite of compositional and structural similarities, have very different electronic structures and magnetic properties. We note also that whereas the study of conventional ferromagnetic (FM) metallic substances employing polarized positrons has been performed by several authors,[25–27,30] NiMnSb is the only half-metal ever studied via 2D-ACAR.[28,29]

We conclude our discussion with UGe_2 which has attracted large attention for the coexistence of magnetic ordering and superconductivity.[33] Due to a strong spin-orbit interaction, which intermixes the spin-up and spin-down channels, the vanishing of the probe effects is less evident here. Nevertheless, we show that the polarized momentum density measurements give fine details compared to the standard nonpolarized ones. Furthermore, we update previous conclusions based on the analysis of the 2D-ACAR experiment performed on UGe_2 in the paramagnetic regime.[34]

A. CrO_2

The metal oxide CrO_2 combines extreme technical importance, as a typical material for magnetic recording, with the riddle of its electronic structure. Indeed, unlike most of the metal oxides, CrO_2 is predicted to be a half-metal by a variety of *ab initio* band-structure calculations.[35–39] Other unusual theoretical result is that different recipes to approximate the exchange-correlation potential V_{xc} [local spin-density approximation[23,24] (LSDA) and generalized gradient approximation[40] (GGA)] lead to noticeable differences in the FS topology and the density of states (DOS) at E_F.[36] This puzzle was not elucidated by measurements of the experimental low-temperature specific-heat coefficients, which showed a spread of values[41,42] even higher than the calculated (DOS)E_F via LSDA or GGA. A measurement of the FS topology is required to clarify this issue. Moreover, Toropova *et al.*[39] have investigated whether methods alternative to the standard LSDA,[24] such as LDA+U,[43] more suited to treat strong electron correlations, could better describe the strong exchange interaction characterizing the half-metals. The comparison of LSDA and LDA+U calculations with x-ray-absorption and ultraviolet photoemission spectroscopy experiments[41,44] showed a clear propensity for the LSDA calculation, making Toropova *et al.*[39] conclude that "the ordered phase of CrO_2 could be described as weakly correlated material with small values of on-site Coulomb repulsion." This apparent contradictory result is discussed by Mazin *et al.*,[36] who noted that LDA+U is superior to LSDA for systems where the local Coulomb interaction (U) is much larger than the band width (W), such as in most metal oxides, in *metallic* CrO_2, where $U/W \simeq 0.5$, the advantages of LDA+U with respect to LSDA are not proven. Similarly, Kuneš *et al.*[38] compared measured magneto-optical Kerr spectra to calculated ones based on LDA, GGA, and LDA+U methods. They concluded that whereas GGA gives qualitatively the best agreement with experiment, LDA+U does not improve results of LDA to any extent.

Concerning experimental confirmations of the half-metallicity, photoemission (PES) experiments have detected a spin polarization of almost 100% 2 eV below the Fermi level E_F but negligible PES intensity at E_F (i.e., insulating behavior[45]). Later experiments performed via PES on standard thin films[46] and on a superconducting junction[47] have updated the PES findings claiming a maximum spin polarization at the Fermi level of $(95 \pm 5)\%$. Nevertheless, the extremely low intensity of the PES signal at E_F (see Fig. 3 of Ref. 46) suggests to pursue the investigation of this system.

The crystal structure of CrO_2 is simple tetragonal [rutile type, space-group $P4_2/mnm$ (Ref. 35)] with 2 f.u. per unit cell. The lattice constants used in the spin-polarized calculations are $a=4.421$ Å and $c=2.916$ Å, respectively. The muffin-tin radii were 1.85 a.u. (1 a.u.$=0.529\,17$ Å) and 1.60 a.u. for Cr and O, respectively. In the interstitial region, the plane-wave expansion was truncated at the maximum wave vector $K_{max} \simeq 4.3$ a.u.$^{-1}$, which gives more than 100 basis functions per atom.

The LCW density was evaluated on a uniform mesh of 1820 **k** points in the irreducible wedge of the first BZ. This corresponds to $25 \times 25 \times 39$ **k** points in the full first BZ. In light of the large dependence of the FS topology on the exchange and correlation potential reported in Ref. 36, both the LDA and GGA exchange-correlation functionals were employed in the calculations. The FS within the LSDA was

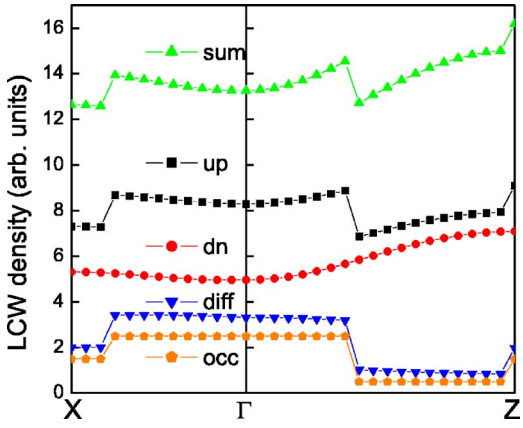

FIG. 1. (Color online) The LCW densities of the up (up) spin, conducting, and down (dn) spin, insulating, spin-polarized states of CrO_2, together with their sum (sum) and difference (diff) along two high-symmetry directions of the Brillouin zone. The occupancy of the up-spin states (occ) is also shown. For the sake of clarity, the occupancy curve is scaled and shifted in the vertical direction.

presented in detail in our previous work (Fig. 1 of Ref. 13) and elsewhere.[36,37] It consists of a Γ centered convex structure denoted as *pseudocube*[36] and a holelike one centered midway between Γ and *Z*. Moreover, there are minuscule parts of the FS denoted as *needles*,[37] which probably could not be detected experimentally.

Interestingly, the topology of the holelike manifold turns out to differ significantly for the two exchange correlation potentials, GGA and LSDA. Whereas in the GGA case, the FS has a simple, pillowlike shape, the FS manifold resulting from LSDA is a pseudosphere connected to a toroidal structure with rhombic shape (see Fig. 1 in Ref. 13). The electronlike and holelike sheets have equal volume. The Fermi volumes resulting from LSDA and GGA differ slightly, corresponding to 12.8% of the BZ and 10.7% of the BZ for LSDA and GGA, respectively.

The self-consistent calculation was performed including spin-orbit coupling at each variational step. The integral in Eq. (2) was evaluated on a regular mesh in the irreducible real-space cell, equivalent to having $84\times84\times55$ points in the whole unit cell. We have carefully checked that with these calculational parameters, all presented results are well converged.

An interesting question is whether 2D-ACAR experiments would be able to reveal the FS of CrO_2 and rule over the different responses of the two exchange-correlation potentials. To investigate this issue, one must evaluate the modulation of the occupancy caused by the non-uniformity of the positron density. This was addressed in our recent publication,[13] where a complete simulation of an experiment has been performed (including realistic positron beam polarization P_{e^+}, experimental resolution, and statistical noise due to finite number of counts). The simulation has proved that the 2D-ACAR experiment can yield the spin density and the fine structure of the Fermi surface. Moreover, it has provided the level of statistical precision required to rule in favor of one or another exchange-correlation potential (see Figs. 3 and 4 in Ref. 4).

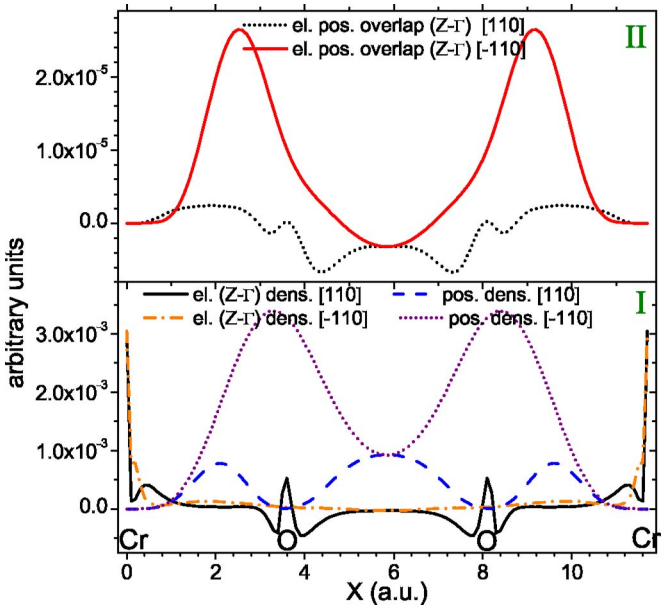

FIG. 2. (Color online) (I) Difference between the electron densities of *Z* and Γ states in CrO_2 along [110], continuous line (black) and [−110], and dash-dotted line (orange) of the (001) plane. Also, the positron density for the same directions (dashed blue and dotted purple) is shown. The letters mark the positions of Cr and O atoms along [110]. (II) Difference between the electron-positron overlap with *Z* and Γ states along [110], dotted line (black) and [−110], and continuous line (red) in the same plane.

To help the reader to appraise the cancellation of positron wave-function effects, Fig. 1 shows a comparison of the LCW density of the up-spin (conducting) and down-spin (insulating) cases, their sum and difference and the occupancy of the up-spin case, along two high-symmetry lines of the Brillouin zone. Strikingly, whereas the up and down LCW densities show a relevant modulation due to the positron wave-function effect, whose amplitude is even increased in the sum of the two LCW densities, the difference spectrum shows an almost complete cancellation of the modulation. Therefore, its **k** dependence is practically identical to the occupancy of the up-spin electrons (shown in the same figure).

We have investigated the strong modulation of the down-spin LCW density along the Γ-*Z* ([001]) direction shown in Fig. 1. The study of the band orbital character of the down-spin bands for energies between 1 and 8 eV below E_F did not show any noticeable **k** dependence of the hybridization. The main character of these bands is oxygen *p* like. The O-*s* bands are located at much lower energies (between 17 and 20 eV below E_F) and have very small dispersion. A simple application of the tight-binding method shows that for a pure *p*-type band, the Γ point is located at the top of the band and is an antibonding state, i.e., more delocalized than states at the bottom of the band which are bonding. Indeed, the band structure of occupied bands (see, for example, Fig. 3 of Ref. 37) has the maximum at Γ, consistent with the pure O-*p* character mentioned above. The plot of the spatial electron densities at *Z* and Γ confirms the larger delocalization of the Γ state. This is shown in Fig. 2 (I), where the difference

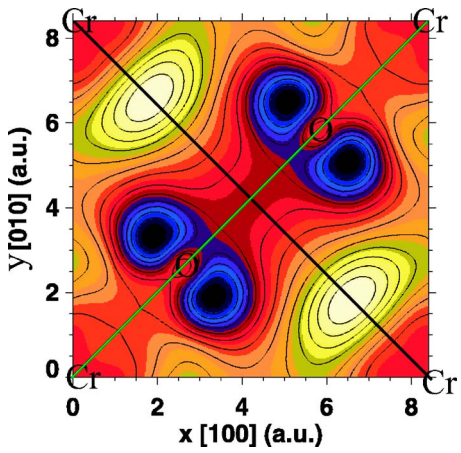

FIG. 3. (Color online) Difference between the electron-positron overlap with Z and Γ states of CrO_2 in the (001) plane. The positions of Cr and O atoms in the plane are shown. The two highlighted diagonals indicate the two directions ([110], [−110]) shown in Fig. 2. Light color corresponds to high intensity and dark color to low intensity.

between the electron densities for Z and Γ states in the (001) plane along the [110] and [−110] directions is plotted (these cuts are also marked as the diagonals of Fig. 3).

The positive peaks of the difference density in proximity of the oxygen and chromium atoms address a higher localization of the Z states compared to the Γ states. These peaks correspond to minima of the positron density (shown in the same figure for the same directions), which, conversely, has, as usual, its maxima in the interstitial region [dashed (blue) line]. We note, however, also a small positive sign of the difference (Z-Γ) in the interstitial region, along [−110], addressing a stronger overlap with the positron for the Z states. The high intensity of the positron density in the interstitial region enhances the small difference of the two electron densities, yielding the pronounced peaks of the difference of the electron-positron overlap along [−110], shown in Fig. 2 (II). Figure 3 shows [at $\simeq$(6.75, 1.75) a.u. and at $\simeq$(1.75, 6.75) a.u.] the large peaks of the aforementioned difference in the whole (001) plane, addressing this peculiar effect. The integral of the difference, which is positive for each plane parallel to (001) of the Wigner-Seitz cell, accounts for the theoretical prediction of the propensity of the positron to sample the Z-type states (consistent with Fig. 1).

Similar considerations hold for the fully occupied bands of the LCW up-spin density. The density of states (see, for example, Fig. 2 of Ref. 36) can also qualitatively explain the cancellation of the probe effects which occurs in CrO_2 after taking the difference among the down and up LCW densities. The oxygen p states form a wide band between −8 and −2 eV (with respect to the Fermi level E_F). As discussed above, they bring a considerable amount of probe effects in $\rho_{par,antipar}(\mathbf{k})$, but in the $\rho^{ep}_{spin}(\mathbf{k})$, they cancel out. The remaining signal is due to Cr-d states, which hybridize only weakly with p states. The stiffness of the d-like bands, having little $\mathbf{k}$ dispersion, causes the modulation due to probe effects to be negligible.

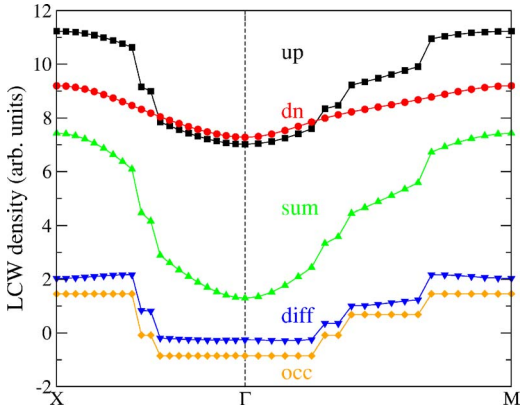

FIG. 4. (Color online) The LCW densities of the up-spin (conducting) and down (dn)-spin (insulating) spin-polarized states of NiMnSb, together with their sum and difference (diff) along two high-symmetry directions of the Brillouin zone. The occupancy of the up-spin states is also shown. For the sake of clarity, the occupancy curve is scaled and shifted in the vertical direction.

B. NiMnSb and Ni_2MnSb

The Heusler alloys form an interesting group of materials, with several half-metals, such having relatively large critical temperatures (NiMnSb, PtMnSb, and CoMnSb).[48,49] The family of Heusler alloys $Ni_{1+x}MnSb$ ($0 \leqslant x \leqslant 1$) is an interesting example because of large differences in the electronic structure and magnetic properties of the two boundary compounds NiMnSb and Ni_2MnSb. NiMnSb is a half-metal with a high Curie temperature of T_C=732 K. Addition of nickel (which is itself ferromagnetic) causes a decrease of T_C down to 368 K for Ni_2MnSb (Ref. 51) (well below the T_C of elemental fcc nickel). Recent theoretical studies of this alloy have proposed a Ruderman-Kittel-Kasuya-Yosida-type behavior of exchange interactions in Ni_2MnSb, which is a standard metallic ferromagnet, as opposed to exponentially damped interactions in the half-metallic NiMnSb.[50]

Positron annihilation studies on NiMnSb have been performed in the pioneering work of Hanssen *et al.*[28,29]

Since our calculation confirmed in full the FS topology shown by Hanssen *et al.* in Fig. 4 of Ref. 28 (consisting of three Γ centered holelike structures), we will concentrate on the differences between occupancies and LCW densities for both spin channels.

Due to the half-metallicity, in NiMnSb, the occupancy of minority-spin channel is constant in $\mathbf{k}$ space. Consequently, in analogy with CrO_2, the up-spin occupancy and the total occupancy (spin-up plus spin-down occupancies) differ from the difference spin-up minus spin-down occupancies (occ in Fig. 4) only by a constant term. The behavior of $\rho^{ep}_{LCWspin}(\mathbf{k})$ is more complex. The $\rho^{ep}_{LCW}(\mathbf{k})$ of spin-down channel does not display any discontinuity, but the modulation of the overlap integral has a larger magnitude than the discontinuities in the spin-up channel. The sum of both spin channels contains even stronger modulations, which (including the finite experimental resolution) can easily overshadow the FS breaks. In particular, since the amplitude of the LCW density along any contour of the FS is modulated by a strong probe effect due to the full bands, any isodensity surface-based method

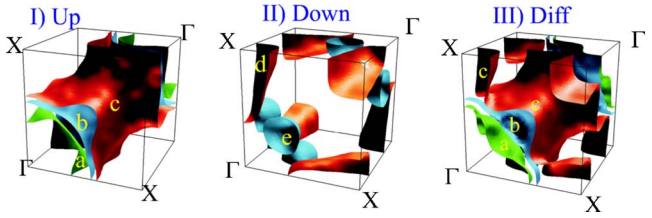

FIG. 5. (Color online) (I) Three majority-spin Fermi-surface sheets of Ni_2MnSb shown in 1/8 of the conventional Brillouin-zone boundaries. (II) The same for the two minority-spin Fermi-surface sheets of Ni_2MnSb. (III) Isodensity surfaces at the average maximum gradient (Ref. 3) of the difference of majority-spin (up)–minority (down)-spin calculated LCW densities.

for reconstruction of the FS would be ineffective.

Conversely, in the difference of spin-resolved momentum densities (similar to the CrO_2 case), most of the modulation disappears and the resulting $\rho^{ep}_{LCWspin}(\mathbf{k})$ is remarkably similar to the occupation shown in Fig. 4. We note that thanks to the half-metallic behavior, $\rho^{ep}_{LCWspin}(\mathbf{k})$ preserves the right character of the FS pockets [electronlike sheets in the occupancy appear as electronlike pocket in the difference $\rho^{ep}_{LCWspin}(\mathbf{k})$; the same happens for the holelike FS]. The almost complete elimination of probe effects, which went unnoticed in Ref. 28, allows a FS reconstruction in terms of isodensity surfaces.

The compound Ni_2MnSb is a ferromagnetic metal with different Fermi surfaces for both spin channels. Therefore, the difference of spin-up and spin-down occupancies varies from the total occupancy not only in a shift by a constant but also in the shape.

The Fermi surface of Ni_2MnSb consists of five sheets. Three for majority-spin channel [Fig. 5 (I)] and two for minority-spin channel [Fig. 5 (II)]. The majority-spin FS sheets are rather similar to the NiMnSb FS sheets. The *b* and *c* sheets (online blue and orange), have octahedral form and enclose tightly the *a* (online green) FS sheet. Both minority spin FS sheets are multiply connected. The *d* (online orange) one consists of six prolate oval electronlike shapes with rounded square cross section at FS boundaries with longer axis along Γ-*X* direction and the *e* one (online blue) consists of 12 holelike balls placed on midpoints of all edges of a cube with edge $\sim\frac{2\pi}{3a}$ around the Γ point.

The majority- and minority-spin momentum densities are shown in the left panel of Fig. 6. Although the modulation of $\rho(\mathbf{k})$ is weaker than what observed in NiMnSb, its amplitude is comparable to the magnitudes of Fermi breaks. In particular, the modulation is relevant in the sum of LCW densities $\rho_{sum}(\mathbf{k})$. On the other hand, the difference $\rho^{ep}_{LCW}(\mathbf{k})$ follows very closely the difference of occupancies with significantly reduced modulation. In Fig. 5 (III), we show the isodensity surfaces of the difference of the up-down LCW densities extracted with the average maximum gradient method.[3] The algorithm is able to separate three FS sheets only. Consistent with the finding of Fig. 6 and unlike what is observed in the two half-metals analyzed so far, the difference mixes the up and down Fermi surfaces. The result is that whereas sheet *a* of panel (I) appears in panel (III) relatively undistorted, sheet *c* of panel (III) has become a combination of sheet *c* from

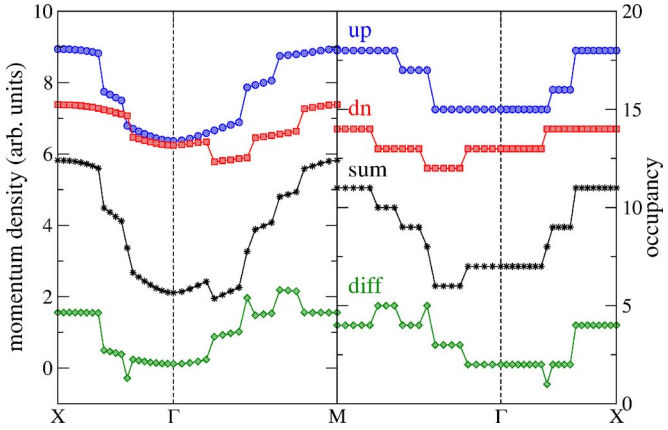

FIG. 6. (Color online) Comparison of LCW density (left panel) and occupancy (right panel) in the Ni_2MnSb along *X*-Γ-*M* path in the Brillouin zone. Blue circles and red squares correspond to majority-spin and minority-spin components, respectively. Black stars and green diamonds correspond to their sum and difference, respectively. For the sake of clarity, spin-up, spin-down, and sum curves are shifted in the vertical direction preserving the relative position of spin-up and spin-down components.

panel (I) and sheet *d* from panel (II). Clearly, the interpretation of the experimental results needs a close comparison with the calculated LCW density difference. In a way, the clear-cut results obtained for the two half-metals are lost. Nevertheless, the main point emphasized in this work, namely, that a large part of the disturbance caused by positron wave-function effects disappears by taking the difference of the LCW densities, is confirmed (as indicated more clearly by Fig. 6).

C. UGe_2

Ferromagnetic UGe_2 is a rare example of pure system endowed of a strong magnetic moment ($\mu=1.4\mu_B$) turning into superconductor at $T<1$ K under a limited pressure range (1–1.6 GPa). Indeed, superconductivity disappears in the paramagnetic region. This finding has suggested the onset of a spin triplet magnetically mediated superconductivity.[33] A natural consequence of this conjecture is that the electrons carrying the magnetic moments should be itinerant at the onset of superconductivity. In Ref. 34, we reported 2D-ACAR experiments on UGe_2 in the paramagnetic phase. The very long *b* axis, $b=15.083$ Å (with the consequent reduction of the BZ along [010]), suggested to acquire the angular correlation spectra with integration direction parallel to [010]. This projection direction was also advantageous to reveal an important cylindrical structure of the FS, lying along the [010] direction as well. Indeed, a critical difference predicted by the theory for the itinerant or localized model of the 5*f* electrons concerned the electronlike or holelike character of this FS sheet. The dHvA technique is unable to detect these differences. Conversely, our findings[34] based on comparing the experimental projected LCW density with the electronic occupancy were clearly supporting the 5*f* localized model (see Fig. 2 of Ref. 34). However, our later experiments of the 5*f*-electron antiferromagnet UGa_3, cor-

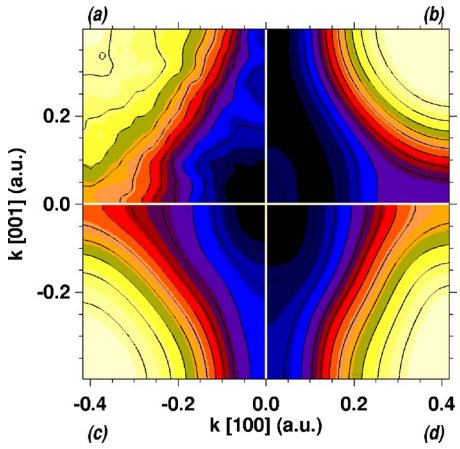

FIG. 7. (Color online) Quadrant (a): 2D $\rho^{ep}_{LCW}(k_x,k_y)$ density of UGe_2 in the paramagnetic phase obtained from LCW folding the 2D experimental projection $\rho^{ep}(p_x,p_y)$, with p_z along the [010] axis. The contour level spacing corresponds to 0.4% of the maximum. Quadrants (b), (c), and (d): Projected FLAPW calculated LCW densities convoluted with the assumed experimental resolution (see text): (b) f-core model, (c) dual-f model (two $5f$ electrons in core), and (d) f-band model. The matrix sizes are equivalent to $2\pi/a \times 2\pi/c$. 1 Bloch wave vector a.u.=1 momentum a.u./$\hbar$=1/a_0 =1.89 Å^{-1}, where a_0 is the Bohr radius.

roborated by the calculations of the LCW density, showed that the modulation of the LCW density due to the nonuniform positron density can be very strong when the character of f electrons is mostly itinerant.[12]

This finding raised the question of the effect of the positron wave function in UGe_2 and whether it could alter the conclusions of Ref. 34. Therefore, we decided to reinvestigate the experimental data comparing the experimental LCW density with the calculated one. As in Ref. 34, the (relativistic) band-structure calculation[19] adopted three ways to treat the $5f$ electrons of uranium. (i) The $5f$ electrons were considered as ordinary band electrons (f band). (ii) The $5f$ electrons were regarded as core states (f core). The f-core calculation was accomplished by forcing a U $5f^3$ core configuration. (iii) Following the guidelines of Ref. 52, we treated only two $5f$ electrons as core electrons (dual f), allowing band $5f$ states to be occupied, i.e., releasing the constraint of the energy parameter for the $5f$ orbital adopted in the open f-core treatment. The resulting total occupancy of f states was 2.7 in this approach.

Figure 7 shows two-dimensional line integrals along the [010] direction of the f-core, dual-f, and f-band calculated LCW densities [quadrants 7(b), 7(c), and 7(d), respectively] compared to the 2D-LCW folded data of the 2D-ACAR measurement for the same projection direction [quadrant 7(a)]. Details of the data acquisition are reported in Ref. 34. The theoretical results of Fig. 7 were convoluted with the experimental resolution [(0.09,0.14) a.u.]. Compared to Fig. 2 of Ref. 34, where the experimental spectrum was compared to the occupancies obtained with the three methods, there are striking differences. Whereas panel 7(b) resembles closely panel (b) of Fig. 2 of Ref. 34, confirming our previous finding that when the f electrons treated as localized positron wave-function effects are modest,[12,18] for the f-band and dual-f cases [panels (c) and (d)], the comparison with the corresponding panels of Fig. 2 of Ref. 34 yields almost opposite results. We recall that the maxima at the edges of the projected BZ of the f-core calculations are caused by integration of an electronlike cylindrical FS. In the f-band calculation, this structure has a similar shape but is holelike (see Figs. 3 and 4 of Ref. 34), leading to a minimum at the edges of the projected BZ. Nevertheless, the positron-wave function effect is so intense to turn this minimum into a maximum. Similar considerations hold for the dual-f case, leading to a projected occupancy radically different from the f-band and f-core calculations [see Fig. 2(c) of Ref. 34] but to a very similar LCW density. These findings demand to reconsider our previous claims. Although in Fig. 7 the shape of the contour lines seems to suggest a small propensity for the f-band or dual-f models, it is clear that our 2D-ACAR measurements are unable to draw conclusions on the f-electron character in the paramagnetic phase of UGe_2.

On the other hand, the strong cancellation of positron wave-function effects predicted for the FM phase of CrO_2 suggests to calculate the net LCW spin density in the FM phase which is easily accessible experimentally (T_C=52 K). Beyond the three theoretical models adopted for the paramagnetic phase (f band, f core, and dual f), we have performed an LSDA+U calculation employing the values of U=0.7 eV and J=0.44 eV optimized in Ref. 53 to reproduce the experimental magnetic moment of 1.4μ_B. We used the same variant of LDA+U method, namely, the *around mean field* LDA+U (Ref. 54) implemented in the WIEN2K code in a rotation invariant way, which includes the spin-off-diagonal terms in the resulting orbital potential. The resulting spin and orbital moments are in excellent agreement with those calculated in Ref. 53. The calculation of $\rho^{ep}_{LCWpar}(\mathbf{k})$ and $\rho^{ep}_{LCWantipar}(\mathbf{k})$ in the four cases shows little difference, owing to the predicted strong positron wave-function effects. All the resulting spectra are remarkably similar to the corresponding spectra obtained in paramagnetic phase, shown in Fig. 7. Therefore, we prefer to show in Fig. 8 (II) only the differences $\rho^{ep}_{LCWpar}(\mathbf{k})-\rho^{ep}_{LCWantipar}(\mathbf{k})$ for the four cases discussed. As for CrO_2 in Ref. 13, we have simulated in full the output of a 2D-ACAR experiment, choosing a positron polarization P_{e^+}=0.35 and a data collection statistics of 4 $\times 10^8$ raw coincidence counts (assuming later to symmetrize the data to quadruplicate the statistics). Figure 8 (I) shows, for the same cases, the difference between the up- and down-spin occupancies, convoluted with the same experimental resolution adopted above (note that no noise propagation was applied in this case). Figure 8 (I) can be considered as the analogous of Fig. 8 (II) in the limit of a constant positron wave function (having preserved the mixing of the up-down electronic states due to spin-orbit coupling). Therefore, the differences between Figs. 8 (I) and 8 (II) are uniquely due to non uniform positron density, whose striking effect can be appraised by comparing Fig. 7 with Fig. 2 of Ref. 34. The agreement between the corresponding panels relating to the open core (a) and dual (c) models is excellent, addressing a strong elimination of positron wave-function effects, which is the main point of our paper. For the two remaining cases (b) and (d), the agreement between panels (I) and (II) is

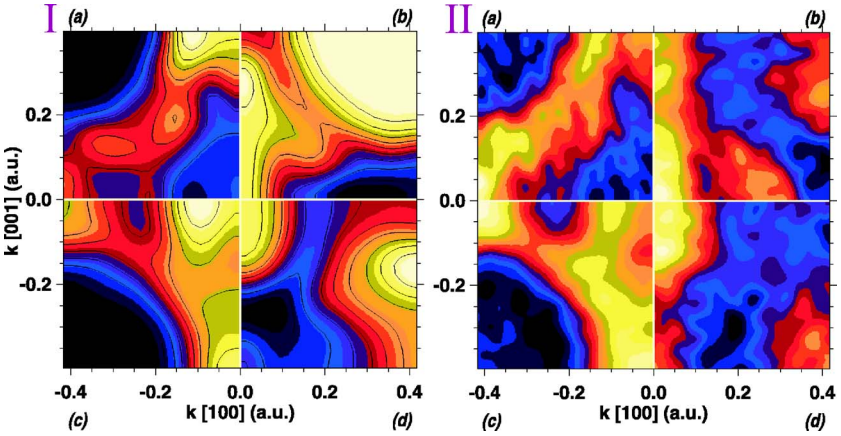

FIG. 8. (Color online) Left (I): Difference between the calculated up down spin occupancies of UGe_2 as described in the text: (a) f-core model, (b) f-band model, (c) dual-f model (two $5f$ electrons in core). (d) LDA+U. Right (II): $\rho^{ep}_{LCWspin}(\mathbf{k})$ calculated for the same cases of left panel (I). The matrix sizes are equivalent to $2\pi/a \times 2\pi/c$.

limited to the central part of the projected BZ (for $|k_x| < 0.05$ a.u.).

In summary, we can observe a considerable reduction of positron wave-function effects, particularly for f-core and dual-f models, due to the difference between the up-down LCW densities. Unlike the case of Fig. 7 where all the calculations yielded very similar spectra, the LCW density differences calculated for the four methods show pronounced differences. Importantly, all the trends shown in Fig. 8 (II) are robust against the propagation of noise (this was tested by applying different noise seeds to all the spectra).

We emphasize that the combination of strong spin-orbit coupling, large unit cell having low symmetry, and strong positron wave-function effects make the study of UGe_2 rather complex. Nevertheless, the accurate use of the theoretical support in the interpretation of the experimental results should establish a propensity toward on or another electron character in the magnetically ordered phase. Note, for example, the large differences between the dual-f calculation[52,55] [Fig. 8 (II)(c)] and the f-band or LSDA+U ones [Figs. 8 (II)(b) and Fig. 8 (II)(d)].

IV. CONCLUSIONS

In conclusion, we have extended our scheme to calculate the electron-positron **k**-space density (LCW density), based on the FLAPW code WIEN2K, to spin-polarized materials. Our calculations included spin-orbit interaction and employed full- potential methods.

We have calculated the LCW densities of the half-metal CrO_2, observing an almost complete cancellation of the modulation of the LCW density caused by nonuniform positron density. This cancellation allows us to reveal the FS in great detail, thus testing different forms of the exchange-correlation potentials (LSDA and GGA) adopted in density-functional theory.

We have observed an analogous effect in the *net spin LCW density* of the half-metal NiMnSb and the related ferromagnetic Heusler compound Ni_2MnSb. These findings prove that the cancellation we have conjectured is not a fortuitous case observed in a particular compound (CrO_2) but can prove to have large applications in a vast class of materials. In this regard, we are considering the requirements which might lead to the same effects in antiferromagnetic or paramagnetic metals under the action of an intense external magnetic field.[56]

Furthermore, we have calculated the net spin LCW density with different models in the FM UGe_2, preceded by a comparison between an early experiment[34] and a calculation in the paramagnetic phase. In both phases, we predict a strong positron wave-function effect. The results obtained in the paramagnetic phase show that the conclusions of our previous paper[34] of $5f$-electron localization have no basis. Indeed, the similarities of the LCW densities for the different models prevent to give a clear preference for one or another model (f band, f core, and dual f).

In contrast, thanks to large eliminations of the positron wave-function effects, the calculation of the net LCW spin density in the FM phase shows important differences between the different models. These differences can be employed to interpret the experimental spectra and rule in favor of one or another model.

ACKNOWLEDGMENTS

We thank Allen Mills and Sandro Massidda for stimulating discussions. Work partly supported by Grant No. DMEA H9400306206042.

*Electronic address: jan.rusz@fysik.uu.se
†Also at ENEA, Via Don Fiammelli 2, 40129 Bologna, Italy.

[1] A. M. Cormack, J. Appl. Phys. **35**, 2908 (1964).
[2] G. Kontrym-Sznajd, Phys. Status Solidi A **79**, 227 (1990).
[3] M. Biasini, G. Ferro, G. Kontrym-Sznajd, and A. Czopnik, Phys. Rev. B **66**, 075126 (2002).
[4] M. Biasini, G. Kontrym-Sznajd, M. A. Monge, M. Gemmi, A. Czopnik, and A. Jura, Phys. Rev. Lett. **86**, 4616 (2001).
[5] M. Biasini, G. Ferro, and A. Czopnik, Phys. Rev. B **68**, 094513 (2003).

[6] S. Kahana, Phys. Rev. **129**, 1622 (1963).
[7] E. Boronski and R. M. Nieminen, Phys. Rev. B **34**, 3820 (1986).
[8] T. Jarlborg and A. K. Singh, Phys. Rev. B **36**, 4660 (1987).
[9] See L. J. Lantto, Phys. Rev. B **36**, 5160 (1987); A. Kallio, P. Pietiläinen, and L. Lantto, Phys. Scr. **25**, 943 (1982); P. Pietiläinen and A. Kallio, Phys. Rev. B **27**, 224 (1983), and references therein.
[10] H. Sorman and D. Wallner, Mater. Sci. Forum **105-110**, 845 (1992).
[11] P. A. Sterne, R. H. Howell, M. J. Fluss, J. H. Kaiser, K. Kitazawa, and H. Kojima, J. Phys. Chem. Solids **54**, 1231 (1993).
[12] J. Rusz, M. Biasini, and A. Czopnik, Phys. Rev. Lett. **93**, 156405 (2004).
[13] M. Biasini and J. Rusz, J. Phys.: Condens. Matter **18**, L289 (2006).
[14] S. Berko, *Proceedings of the International School of Physics Enrico Fermi*, edited by W. Brandt and A. Dupasquier (North-Holland, Amsterdam, 1983), p. 64.
[15] E. Boronski and R. M. Nieminen, Phys. Rev. B **34**, 3820 (1986).
[16] D. G. Lock, V. H. Crisp, and R. N. West, J. Phys. F: Met. Phys. **3**, 561 (1973).
[17] J. H. Kaiser, R. N. West, and N. Shiotani, J. Phys. F: Met. Phys. **16**, 1307 (1986).
[18] J. Rusz and M. Biasini, Phys. Rev. B **71**, 233103 (2005).
[19] P. Blaha, K. Schwarz, G. K. H. Madsen, D. Kvasnicka, and J. Luitz, WIEN2K, Vienna University of Technology, 2000.
[20] D. Singh, W. E. Pickett, E. C. von Stetten, and S. Berko, Phys. Rev. B **42**, R2696 (1990).
[21] H. Stachowiaka and E. Boronski, Acta Phys. Pol. A **107**, 541 (2005).
[22] See, for example, B. Barbiellini, M. J. Puska, T. Korhonen, A. Harju, T. Torsti, and R. M. Nieminen, Phys. Rev. B **53**, 16201 (1996).
[23] P. Hohenberg and W. Kohn, Phys. Rev. **136**, B864 (1964); W. Kohn and L. J. Sham, Phys. Rev. **140**, A1133 (1965).
[24] R. O. Jones and O. Gunnarson, Rev. Mod. Phys. **61**, 689 (1989) and references therein.
[25] S. Berko and A. P. Mills, J. Phys. (Paris), Colloq. **32**, C1–287 (1971).
[26] P. Genoud, A. K. Singh, A. A. Manuel, T. Jarlborg, E. Walker, M. Peter, and M. Weller, J. Phys. F: Met. Phys. **18**, 1933 (1988).
[27] P. Genoud, A. A. Manuel, E. Walker, and M. Peter, J. Phys.: Condens. Matter **3**, 4201 (1991).
[28] K. E. H. M. Hanssen and P. E. Mijnarends, Phys. Rev. B **34**, 5009 (1986).
[29] K. E. H. M. Hanssen, P. E. Mijnarends, L. P. L. M. Rabou, and K. H. J. Buschow, Phys. Rev. B **42**, 1533 (1990).
[30] T. Chiba, J. Chem. Phys. **64**, 1182 (1976).
[31] See, for example, J. J. Sakurai, *Advanced Quantum Mechanics* (Addison-Wesley, Reading, MA, 1967), pp. 93 and 113.
[32] Note that introducing N^{NM}, is not strictly necessary. However, we find it instructive to split the $\rho(\mathbf{p})$ into a magnetic and essentially nonmagnetic part which, as it will be shown later, is responsible for most of the probe effects but vanishes when taking the difference between up and down momentum densities.
[33] S. S. Saxena, P. Agarwal, K. Ahilan, F. M. Grosche, R. K. W. Haselwimmer, M. J. Steiner, E. Pugh, I. R. Walker, S. R. Julian, P. Monthoux, G. G. Lonzarich, A. Huxley, I. Sheikin, D. Braithwaite, and J. Flouquet, Nature (London) **406**, 507 (2000) and references therein.
[34] M. Biasini and R. Troc, Phys. Rev. B **68**, 245118 (2003).
[35] P. Sorantin and K. Schwarz, Inorg. Chem. **31**, 567 (1992).
[36] I. I. Mazin, D. J. Singh, and C. Ambrosch-Draxl, Phys. Rev. B **59**, 411 (1999).
[37] N. E. Brener, J. M. Tyler, J. Callaway, D. Bagayoko, and G. L. Zhao, Phys. Rev. B **61**, 16582 (2000).
[38] J. Kuneš, P. Novák, P. M. Oppeneer, C. König, M. Fraune, U. Rüdiger, G. Güntherodt, C. Ambrosch-Draxl, Phys. Rev. B **65**, 165105 (2002).
[39] A. Toropova, G. Kotliar, S. Y. Savrasov, and V. S. Oudovenko, Phys. Rev. B **71**, 172403 (2005).
[40] J. P. Perdew, K. Burke, and M. Ernzerhof, Phys. Rev. Lett. **77**, 3865 (1996).
[41] T. Tsujioka, T. Mizokawa, J. Okamoto, A. Fujimori, M. Nohara, H. Takagi, K. Yamaura, and M. Takano, Phys. Rev. B **56**, R15509 (1997).
[42] N. Schubert and E. Wassermann (unpublished); data quoted in H. Brändle, D. Weller, S. S. P. Parkin, J. C. Scott, P. Fumagalli, W. Reim, R. J. Gambino, R. Ruf, and G. Güntherodt, Phys. Rev. B **46**, 13889 (1992).
[43] V. I. Anisimov, F. Arystiawan, and A. I. Lichtenstein, J. Phys.: Condens. Matter **9**, 767 (1997).
[44] E. Z. Kurmaev, A. Moewes, S. M. Butorin, M. I. Katsnelson, L. D. Finkelstein, J. Nordgren, and P. M. Tedrow, Phys. Rev. B **67**, 155105 (2003).
[45] K. P. Kämper, W. Schmitt, G. Güntherodt, R. J. Gambino, and R. Ruf, Phys. Rev. Lett. **59**, 2788 (1987).
[46] Yu. S. Dedkov, M. Fonine, C. König, U. Rdiger, and G. Güntherodt, Appl. Phys. Lett. **80**, 4181 (2002).
[47] J. S. Parker, S. M. Watts, P. G. Ivanov, and P. Xiong, Phys. Rev. Lett. **88**, 196601 (2002).
[48] R. A. de Groot, F. M. Mueller, P. G. van Engen, and K. H. J. Buschow, Phys. Rev. Lett. **50**, 2024 (1983).
[49] R. A. de Groot, F. M. Mueller, P. G. van Engen, and K. H. J. Buschow, J. Appl. Phys. **55**, 2151 (1984).
[50] J. Rusz, L. Bergqvist, J. Kudrnovský, and I. Turek, Phys. Rev. B **73**, 214412 (2006).
[51] P. J. Webster and R. M. Mankinar, J. Magn. Magn. Mater. **42**, 300 (1984).
[52] G. Zwicknagl, A. N. Yaresko, and P. Fulde, Phys. Rev. B **65**, 081103(R) (2002).
[53] A. B. Shick and W. E. Pickett, Phys. Rev. Lett. **86**, 300 (2000).
[54] M. T. Czyzyk and G. A. Sawatzky, Phys. Rev. B **49**, 14211 (1994).
[55] A. Yaouanc, P. Dalmas de Reotièr, P. C. M. Gubbens, C. T. Kaiser, A. A. Menovsky, M. Mihalik, and S. P. Cottrell, Phys. Rev. Lett. **89**, 147001 (2002).
[56] This suggestion has been provided by Allen Mills, Jr.